Journal of Peptide Science
J. Peptide Sci. 2006; **12**: 161–170
Published online 23 August 2005 in Wiley InterScience (www.interscience.wiley.com). DOI: 10.1002/psc.708

JOURNAL OF PEPTIDE SCIENCE

A short PNA targeting coxsackievirus B3 5′-nontranslated region prevents virus-induced cytolysis

DOMENICA MUSUMECI,[a] MARGHERITA VALENTE,[a] DOMENICA CAPASSO,[a] ROSANNA PALUMBO,[a] MATTHIAS GÖRLACH,[b] MICHAELA SCHMIDTKE,[c] ROLAND ZELL,[c] GIOVANNI N. ROVIELLO,[a] ROBERTO SAPIO,[a] CARLO PEDONE[a] and ENRICO M. BUCCI[a]*

[a] Istituto di Biostrutture e Bioimmagini, CNR, I-80134 Naples, Italy
[b] Abteilung Molekulare Biophysik/NMR-Spektroskopie, Institut für Molekulare Biotechnologie, D-07745 Jena, Germany
[c] Institut für Virologie und Antivirale Therapie, Friedrich-Schiller-Universität, D-07745 Jena, Germany

Received 20 May 2005; *Accepted 4 July 2005*

Abstract: Targeting regulatory RNA regions to interfere with the biosynthesis of a protein is an intriguing alternative to targeting a protein itself. Regulatory regions are often unique in sequence and/or structure and, thus, ideally suited for specific recognition with a low risk of undesired side effects. Targeting regulatory RNA elements, however, is complicated by their complex three-dimensional structure, which poses kinetic and thermodynamic constraints to the recognition by a complementary oligonucleotide. Oligonucleotide mimics, which shift the thermodynamic equilibrium towards complex formation and yield stable complexes with a target RNA, can overcome this problem. Peptide nucleic acids (PNA) represent such a promising class of molecules. PNA are very stable, non-ionic compounds and they are not sensitive to enzymatic degradation. Yet, PNA form specific base pairs with a target sequence. We have designed, synthesised and characterised PNA able to enter infected cells and to bind specifically to a control region of the genomic RNA of coxsackievirus B3 (CVB3), which is an important human pathogen. The results obtained by studying the interaction of such PNA with their RNA target, the entrance into the cell and the viral inhibition are herein presented.

Keywords: 3C protease; coxsackievirus B3; PNA; rhinovirus; viral RNA

INTRODUCTION

The traditional antisense approach consists in targeting an mRNA by antisense oligonucleotides in order to shut off the translation of a selected gene [1]. Even though this approach may look straightforward, some limitations hamper the potential use of antisense oligonucleotides as drug, among them stability to degradation by serum enzymes and the complex folding of potential RNA targets. Besides enzymatic stability, which can be easily improved by using compounds with chemical modifications (e.g. phosphorothioates [2]), a major improvement is expected by using compounds that form a complex with a target RNA more stable than natural oligonucleotides do. In fact, this approach might be the only antisense strategy available when taking into account the high propensity of the RNA to adopt a complex three-dimensional fold [3]. This is the case if one chooses to target a regulatory RNA sequence, since its three-dimensional structure often plays an important role in the functioning of such regions.

PNA are particularly well-suited candidates for binding to such RNA structures and provide means to target a regulatory region in the genome of an RNA virus. Indeed, the superior affinity of PNA for natural oligonucleotides provides a favourable energetic push towards the denaturation of the target RNA, which is required both for the antisense to bind its target [3] and also to interfere with regulatory protein binding. Moreover, PNA are resistant to enzymatic degradation, non-ionic and non-toxic, thus representing excellent candidates for drug development [4]. Last, but not least, the flexible chemistry that is used for PNA synthesis allows for a number of chemical modifications, which in turn have been introduced to enhance cell-delivery, solubility and activity of these compounds [5–8].

Since the life cycle of many RNA viruses is based on the correct functioning of extensive non-translated RNA regions, [9–14] we decided to use PNA to block such an RNA region. Among RNA viruses, the picornaviruses represent good candidates for using PNA as antiviral agent, since the viral life cycle is based on the correct folding and protein recognition of a very long 5′-non-translated (5′-NTR) region [15,16]. Moreover, the picornavirus family contains several human pathogens, including human rhinoviruses

Abbreviations: 3C Protease ($3C^{pro}$); benzhydryloxycarbonyl (Bhoc); *tert*-butoxycarbonyl (Boc); Cytopathic effect assay (CPE assay); Coxsackievirus B3 (CVB3); *N*,*N*-diisopropylethylamine (DIPEA); *N*,*N*-dimethylformamide (DMF); fluorescein-5-isothiocyanate (FITC); fluorenyl-9-methoxycarbonyl (Fmoc); *O*-(7-azabenzotriazol-1-yl)-1,1,3,3-tetramethyluronium hexafluorophosphate; (HATU); 2-(1H-benzotriazol-1-yl)-1,1,3,3-tetramethyluronium hexafluorophosphate (HBTU); 1-hydroxybenzotriazole (HOBt); *N*-methylpyrrolidone (NMP); Peptide nucleic acids (PNA); Stemloop D (SLD); trifluoroacetic acid (TFA).

*Correspondence to: E. M. Bucci, Istituto di Biostrutture e Bioimmagini, CNR, Via Mezzocannone 16, 80134 Napoli, Italy;
e-mail: bucci@chemistry.unina.it

(HRV), human polioviruses (PV), hepatitis A virus (HAV) and coxsackieviruses (CV) [17].

These RNA viruses translate their genetic information into a poly-protein precursor, which is further processed by two viral proteases designated 2A and 3C. The $3C^{pro}$ catalyses most of the internal cleavages. Owing to its unique structure and essential roles in viral replication, $3C^{pro}$ has been viewed as an excellent target for antiviral intervention. As a consequence, considerable efforts have been made in the development of antiviral compounds targeting this protease [18,19].

However, $3C^{pro}$ is a multi-functional protein involved also in viral genome replication [20,21]. Consequently, in parallel with the inhibition of its proteolytic activity, it is also conceivable to block some other important activities of the protein, so as to increase the arsenal of available drugs and the effectiveness of antiviral treatments.

The non-proteolytic functions of $3C^{pro}$ involve the recognition of a specific RNA element (the Stemloop D, (SLD)) located in a cloverleaf structure in the aforementioned 5′-NTR of the viral genome. Using CVB3 as a model system, we have previously shown that there is a specific recognition mechanism between $3C^{pro}$ and SLD, which crucially relies on the RNA structure [22,23]. This result provided the basis for the design of a first generation of inhibitory PNA molecules intended to enter infected human cells, to bind to the target RNA and to inhibit the viral life cycle.

MATERIALS AND METHODS

PAL-PEG-PS resin was purchased from Perseptive Biosystem (Hamburg, Germany). 1-Hydroxybenzotriazole (HOBt), 2-(1H-benzotriazol-1-yl)-1,1,3,3-tetramethyluronium hexafluorophosphate (HBTU) and fluorenyl-9-methoxycarbonyl–Lys (*tert*-butoxycarbonyl)-OH ((Fmoc)–Lys (Boc)-OH) were from Novabiochem (Darmstadt, Germany). PNA monomers, reagents and solvents were purchased from PRIMM (Milan, Italy). Fluorescein-5-isothiocyanate (FITC) (isomer I) and trifluoroacetic acid (TFA) were from Fluka (Steinheim, Germany). Acetonitrile for HPLC chromatography was from Reidel-deHaën (Seelze, Germany), while dry *N*,*N*-dimethylformamide (DMF) and *N*-methylpyrrolidone (NMP) for manual solid-phase synthesis were purchased from LabScan (Dublin, Ireland).

The solid support functionalization was carried out in a short PP column (1.5 ml) equipped with a PTFE filter, a stopcock and a cap. Solid-phase synthesis was performed on an Expedite 8900 Nucleic Acid Synthesis System ABI (Foster City, CA).

Products were purified and analysed with a HPLC system using a Phenomenex Jupiter C18 300 Å column (5 µm, 4.60 × 250 mm) (Phenomenex, Torrance, CA).

MALDI-TOF mass spectrometry was performed on a PerSeptive Biosystems Voyager-MALDI-TOF mass spectrometer (Framingham, MA) using sinapinic acid as matrix and bovine insulin as internal standard.

Electrospray mass-spectra (ESMS) were recorded with API 100 single quadrupole (Perkin Elmer Applied Biosystem Inc., Foster City, CA) mass spectrometer.

K-$(PNA)_{12}$-K Design, Synthesis and Purification

A PNA sequence targeting the selected RNA was identified by checking by BLAST in the EMBL sequence database [24] for:

1. absence of the selected sequence in the human and CVB3 genome (homology threshold: 50%);
2. absence of the complementary sequence in the human and CVB3 genome (homology threshold: 50%);
3. absence of the inverse sequence in the human and CVB3 genome (homology threshold: 50%);
4. absence of the inverse complementary sequence in the human and CVB3 genome (homology threshold: 50%).

For inverse sequence, we mean here the sequence read from the 3′ to the 5′ orientation. The absence of such a sequence in the target genome had to be checked because of the PNA ability to form parallel-oriented double helices. Any candidate PNA sequence was then checked by the software MFOLD [25] for the ability to form self-complementary secondary structures.

The designed K-$(PNA)_{12}$-K was subsequently synthesised using Fmoc chemistry on a PAL-PEG-PS resin (25 mg, 160 µ mol/mg) on a 4 µ moles scale. Both Lys residues were attached manually using HBTU/HOBT/DIPEA in DMF as the C-activator system.

The synthesis yielded *ca* 8.4 mg (≈60% yield) of K-PNA_{12}-K oligomer with a purity of >95% after RP-HPLC purification. The identity of the product was checked by MALDI-TOF (expected MH^+: 3535.12; observed MH^+: 3536.78) and electrospray (observed MH^+: 3534.66).

A scrambled PNA molecule (named K-scrPNA_{12}-K) was also designed using the same principles and obtained by the same procedures. The selected sequence is H-Lys-gacaacattgcg-Lys-NH_2.

The synthesis yielded *ca* 6.9 mg (≈49% yield) of K-scrPNA_{12}-K oligomer with a purity of >95% after RP-HPLC purification. The identity of the product was checked by MALDI-TOF (expected MH^+: 3535.12; observed MNa^+: 3557.26).

FITC-β-Ala-K-$(PNA)_{12}$-K Design, Synthesis, Purification and Characterisation

We label K-$(PNA)_{12}$-K with FITC in solid phase. To perform the solid-phase reaction between K-$(PNA)_{12}$-K and FITC, it was necessary to add a β-Ala on the pseudo-5′-position because the subsequent cleavage and deprotection of PNA from the solid support with TFA can cause Edman degradation in presence of an α-aminoacid residue (Lys) on the 5′ end.

The K-PNA_{12}-K portion was synthesised, as described before, on solid phase on a 4 µ mol scale. The last Lys (on pseudo-5′ position) was N^{α}-deprotected from the Fmoc group and the reaction with β-Ala was performed under the same conditions as those of the last Lys. A solution of FITC (8 eq) in DMF (300 µl) was added to a suspension of H-β-Ala-Lys-PNA_{12}-Lys-R resin in DMF (300 µl) and *N*,*N*-diisopropylethylamine (DIPEA) (3eq). FITC coupling was repeated twice, and then cleavage and deprotection were carried out by treating the resin with a 4 : 1 v : v TFA/*m*-cresol

solution. The surnatant was then treated with cold ethyl ether and dried, and the crude, yellow pellet was dissolved in H_2O (0.1% TFA), purified by RP-HPLC and characterised by MALDI-TOF (expected MH^+: 3994.51; observed MH^+: 3996.35). The amount of recovered FITC-β-Ala-K-PNA_{12}-K was 8.8 mg (55% yield).

RNA and 3C Protease Production

CVB3 SLD RNA was *in vitro* transcribed and purified as previously described [9,23]. $3C^{pro}$ was recombinantly expressed in *Escherichia coli* and purified as previously described [9].

Circular Dichroism

All CD spectra were collected on a Jasco J710 spectropolarimeter equipped with a NesLab RTE111 thermal controller unity, using a quartz cylindrical cuvette with a 1-cm path length (Jasco). We always used a scan speed of 20 nm/min, a bandwidth of 1 nm and a resolution of 1 nm.

In a first experiment, an RNA sample of concentration 1.15 μM in 100 mM phosphate buffer, pH 7.0, was prepared. CD spectra were collected subsequently at increasing PNA concentrations, ranging from 0 to 4.48 μM, in a 200–340 nm spectral window and keeping the temperature constant at 25 °C.

In a second experiment, a sample A1 containing 1.20 μM RNA and a sample A2 containing 1.28 μM PNA and 1.15 μM RNA in 100 mM phosphate buffer, pH 7.0, were prepared. The CD at 257 nm was monitored by increasing the temperature from 20 to 90 °C, with a temperature gradient of 1 °C min^{-1}.

In a third experiment, we prepared a solution of RNA at a concentration of 1.2 μM in 5 mM phosphate buffer, pH 7.0. This solution was split in two identical aliquots (B1 and B2). The CD spectra of B1 and B2 were collected ranging from 200 to 320 nm and keeping the temperature constant at 25 °C. We then added a PNA aliquot to B1 as to get a final PNA concentration of 2.56 μM, and a protein aliquot to B2 as to get a final protein concentration of 1.62 μM. The CD spectra of B1 and B2 were again collected under the same conditions. Finally, we added a protein aliquot to B1 as to get a final protein concentration of 1.62 μM and we repeated the CD measurements under the same conditions.

All concentrations used were determined spectrophotometrically by assuming molar extinction coefficients at 260 nm of 285 100 L cm^{-1} mol^{-1} and 126 900 L cm^{-1} mol^{-1} for RNA and PNA, respectively, as derived from the PerSeptive Biosystems Expedite™ synthesizer user's guide. For the protein, a molar extinction coefficient at 280 nm of 13 490 L cm^{-1} mol^{-1} was assumed [26].

Electrophoretic Mobility Shift Assay

For band shift experiment, we used our previously reported protocol [9]. The samples were applied to native 12% preparative PAA gel electrophoresis. Gels were run for about 20 h at 40 V. After electrophoresis, RNA was stained with ethidiumbromide and visualized by UV light.

Cytotoxicity and CPE Inhibition Assays

In these experiments the cytotoxic and the antiviral effects were quantified using a crystal violet uptake assay, as described elsewhere [27]. This standardised high-throughput assay allows primary antiviral screenings with CVB3 (it has been established with the same sensitivity and reproducibility as the plaque reduction assays, but it is more objective and rapid). All of the experiments were carried out in two-days old confluent cell monolayers incubated at 37 °C in a humidified atmosphere with 5% CO_2.

Briefly, a concentrated solution of each PNA was prepared in sterile water (stock solutions). Aliquots from the stock solutions were then dissolved in Eagle's minimal essential medium (MEM/E; SIGMA No: M-0643), as to let the concentration range from 0.008 to 20 μM, (0.008, 0.015, 0.313, 0.625, 1.25, 2.5, 5, 10 and 20 μM respectively). Each concentration was tested in triplicate. After the aspiration of the cell growth medium, 50 microl of PNA solution in test medium were added.

In the CPE inhibition assay, the PNA aliquots were added immediately before viral infection. Six wells of non-infected and six wells of infected cells without the PNA served as cell and virus control, respectively, on each plate. To calibrate the assay, the 50 and 100% plaque inhibitory concentrations of guanidinium chloride (each three wells) were included as positive control in each microtiter plate. The effect of PNA was assessed after 24 h.

Cell Culture for Fluorescence Measurements

HeLa cells were cultured as exponentially growing subconfluent monolayer on 100 mm plates at 37 °C in a 5% CO_2 air atmosphere in D-MEM supplemented with 10% (v/v) FCS, 1% L-glutamine, 1% penicillin/streptomycin (Invitrogen–Life Technology, Carlsbad, CA).

Fluorescence Microscopy

HeLa cells were seeded into six-well plates on a glass coverslip at a density of 3×10^5 cells/well. After 24 h, the medium was removed and replaced with fresh medium containing K-$(PNA)_{12}$-K FITC 2 μM (control cells received medium with FITC 2 μM). After another 24 h cells on coverslips were washed once with PBS, fixed for 10 min with 3% (w/v) paraformaldehyde in PBS, washed three times in PBS, incubated for 10 min with PBS containing Hoechst 33 258 (1 μg/ml), and finally washed three times with PBS. The coverslips were inverted and mounted in mowiol on glass slides. Slides were analysed using a fluorescent microscope, (Leica DM LB, Deerfield, IL). Significant fields were captured using a IM500 system (Leica).

Phase-contrast Microscopy

HeLa cells were treated as described in the previous section, but after PBS washing they were directly imaged using a combined fluorescence/phase-contrast microscope (Nikon TE2000-U, Tokyo, Japan). Significant fields were captured using the software Eclipse SENET (Nikon).

RESULTS AND DISCUSSION

Target Sequence Selection, PNA Design and Synthesis

The target RNA sequence and its secondary structure are presented in Figure 1(A). The hairpin structure

depicted corresponds to the terminal part of SLD, which, as discussed above, is part of the 5′-non-translated cloverleaf structure at the 5′ of the genome of CVB3.

For the design of a suitable PNA antisense, the following constraints were considered:

1. a sequence length longer than 10 nucleotides, to ensure sufficient affinity and specificity for the target RNA;
2. the absence of competitor target sequences in the human genome;
3. the lack of self-complementarity.

Choosing to synthesise a 12-mer PNA satisfied the first constraint. Selecting a sequence that has no significant similarity to any sequence contained within the human genome, nor is significantly complementary to any other both in parallel and antiparallel orientations, met the second constraint. Finally, we selected a sequence that is not self-complementary, a crucial point in using antisense PNA since PNA/PNA hybrids have a greater stability than any other PNA/oligonucleotide complex [28].

The final PNA sequence, named K-$(PNA)_{12}$-K, is shown in Figure 1(B). Two Lys residues were added to the *N*- and *C*-termini of the antisense PNA to improve its solubility and cellular uptake. Owing to the solid support used for the synthesis, the *C*-terminal Lys carries an amide at its *C*-terminus. HPLC runs showed that the three PNA molecules synthesized are >95% pure (Figure 2).

SLD Binding and Protein Competition

As previously shown [23], the conformation of the SLD is a critical determinant for the interaction of this RNA with the viral protease $3C^{pro}$. The designed K-$(PNA)_{12}$-K has the ability to profoundly alter the 3D-structure of the target RNA upon binding. In this respect, CD spectroscopy represents the ideal technique to monitor

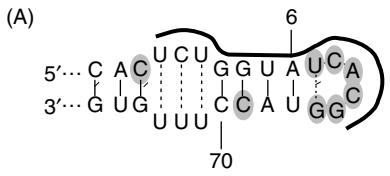

Figure 1 (A) Selected RNA target sequence. The bases shown to be important for 3C binding are shaded gray. The selected PNA target sequence is marked by a thick black line. (B) Designed antisense PNA. The sequence is shown from the *N*- to the *C*-terminus following the convention adopted for peptides. A Lys residue was added at each end. The PNA was designed to interact antiparallel with respect to the RNA.

the formation of the K-$(PNA)_{12}$-K:RNA complex and the accompanying changes in the RNA structure.

Thus, the interaction between SLD and K-$(PNA)_{12}$-K was studied by performing a CD quantitative titration to determine the apparent K_d. A series of spectra was recorded for samples containing K-$(PNA)_{12}$-K:RNA at molar ratios ranging from 0 to 3.9 and at pH 7.0 (Figure 3A).

The formation of the complex was investigated by following the changes in the total spectral area of the 200–340 region, so as to avoid any arbitrary wavelength selection. However, fitting the data at a single wavelength (for example, 257 nm) does not cause significant changes in the K_d value ($K_d = 11.6 \pm 31 \cdot 10^{-9}$ M to be compared with the value of $46.7 \pm 35.5 \cdot 10^{-9}$ M obtained by using the total area).

Here, it is important to note that K-PNA_{12}-K at a concentration equal to the used SLD concentration was found not to significantly contribute to the CD spectra between 220 and 340 nm (figure 3A, dashed red line).

In particular, to estimate the apparent dissociation constant of the K-$(PNA)_{12}$-K:RNA complex, the integral of the CD spectrum between 220 and 340 nm at a given K-$(PNA)_{12}$-K concentration

$$\int_{220}^{340} \text{CD}\, d\lambda = \text{area of the CD spectrum comprised between 220 and 340 nm}$$

was measured and normalised to calculate the fractional saturation values (f). The obtained f values were plotted *versus* the total PNA concentration and fitted by the binding isotherm, as reported in Figure 3(B) [29]. By this method, an apparent dissociation constant of 4.67×10^{-8} M was obtained.

Further data on the complex were derived by considering the specific intensity changes observed in the CD spectrum of RNA upon K-$(PNA)_{12}$-K addition. Changes were observed mainly at 220, 260 and 290 nm, respectively.

The enhancement at 260 nm is consistent with the formation of new double-helical regions, with an overall increase in the stacking of the bases [30].

The decrease of the band centred at 290 nm is consistent with changes in the non-canonically structured regions in SLD, i.e. in the internal bulge and in the apical loop [30].

Finally, the increase at 220 nm can be interpreted as a consequence of the generation of single-stranded regions, most likely due to the opening of the RNA structure by PNA [30].

The thermal stability of the K-$(PNA)_{12}$-K:RNA complex was compared with the stability of SLD by monitoring the corresponding CD spectra at increasing temperatures. The melting profiles obtained by plotting the CD values at 257 nm *versus* the temperature are shown in Figure 4.

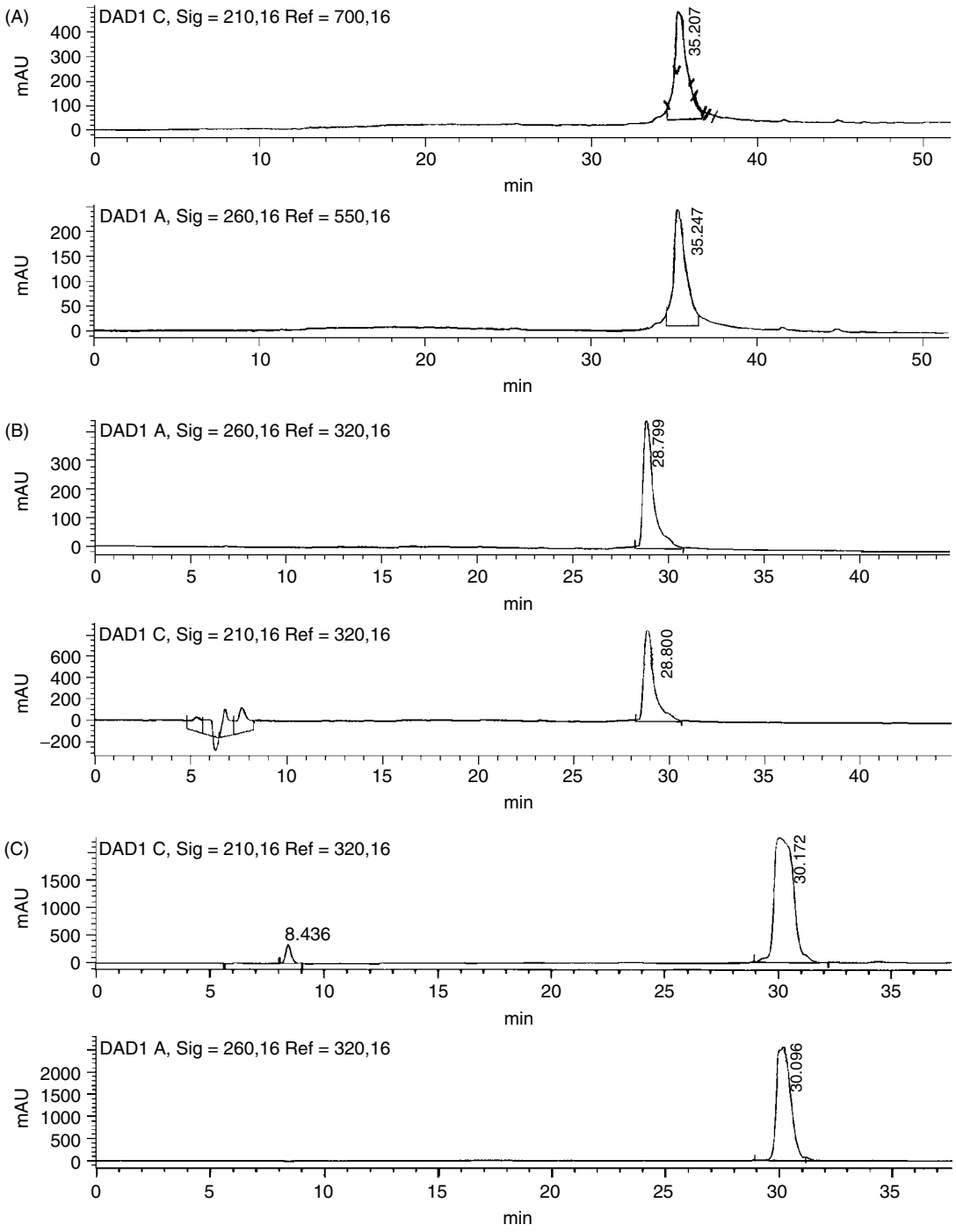

Figure 2 (A) RP-HPLC of purified K-(PNA_{12})-K. 210 and 260 nm profile are shown. (B) RP-HPLC of purified K-scrPNA_{12}-K. Two hundred and ten and 260 nm profile are shown. (C) RP-HPLC of purified FITC-β-Ala-K-(PNA_{12})-K. Two hundred and ten and 260 nm profile are shown.

The K-$(PNA)_{12}$-K : RNA complex has a T_m considerably higher when compared to the T_m of the stemloop D alone, with a shift of about +15 °C. This result highlights the higher stability of the complex. Moreover, the overall melting process of the complex is monophasic, as opposed to the melting of the native SLD (a biphasic process).

The disappearance of the first thermal transition in the SLD melting upon PNA addition, like the decrease of the 290 nm band in the CD spectrum of the complex, is related to the disruption of the non-canonical *intra* molecular interactions in SLD.

The changes induced by the $3C^{pro}$ on RNA structure in the presence or in the absence of K-$(PNA)_{12}$-K were also investigated. The changes in the CD spectrum induced by protein binding to SLD are shown in Figure 5(A). Changes below 240 nm are not informative, since the protein and RNA spectra overlap in this region.

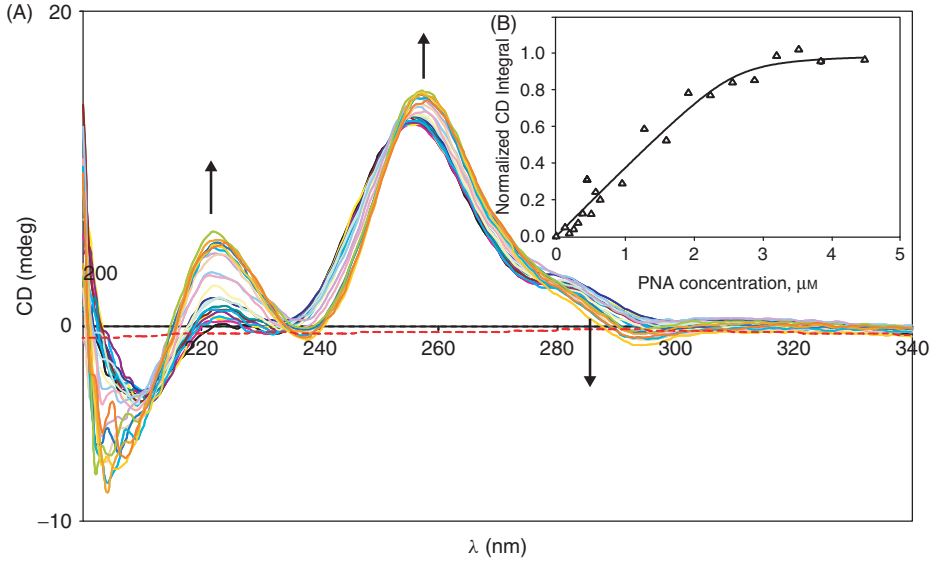

Figure 3 (A) CD-monitored titration of stemloop D with K-$(PNA)_{12}$-K. The arrows mark the most significant changes in the CD spectra of the RNA as the PNA concentration is increased. The dashed red spectrum corresponds to the CD spectrum of the K-$(PNA)_{12}$-K free in solution and at the same concentration of stemloop D (1.15 μM). (B) Titration curve as obtained by plotting the normalized CD integrals *versus* the PNA concentration.

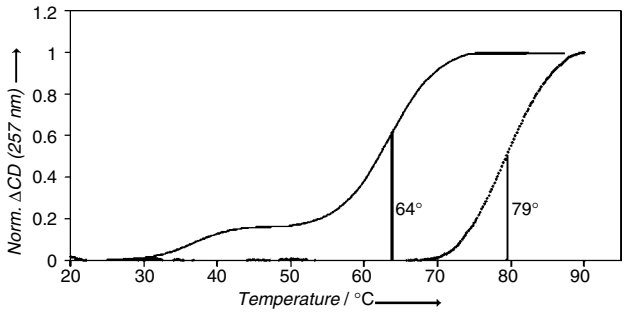

Figure 4 CD-monitored melting profiles of SLD (continuous line) and the K-$(PNA)_{12}$-K : SLD complex (dotted line).

However, the decrease around 260 nm, where only RNA contributes, reflects a change in the environment of the bases upon protein binding. These changes are compatible with changes in the stacking and electronic properties of the bases caused by the protein. When K-$(PNA)_{12}$-K is present (Figure 5B), such protein-induced changes are not observed. Their absence excludes the formation of a native SLD:$3C^{pro}$ complex in presence of K-$(PNA)_{12}$-K.

To exclude an interaction of the 3C proteinase with the RNA/PNA complex, i.e. the formation of a ternary complex, we performed an EMSA as described previously [9,22]. This experiment indicated the formation of the same PNA/RNA complex, irrespective of whether the PNA was added to the RNA in the presence or in the absence of the protein (data not shown). The scrambled PNA sequence H-Lys-gacaacattgcg-Lys-NH_2 was also tested. This PNA did not show any binding to SLD nor any $3C^{pro}$ binding inhibition.

Cytotoxicity and Viral Inhibition Assays

To evaluate both the cytotoxicity and the antiviral activity of K-$(PNA)_{12}$-K, we performed a series of crystal violet uptake assays, as described elsewhere [27], using HeLa cells. The results are reported in Figure 6.

As evident from Figure 6(A), we did not find any detectable cytotoxic effect of the PNA for concentrations of up to 25 μM when compared to untreated cells. Subsequently, the cells were challenged with a standard dose of CVB3 and increasing amounts of K-$(PNA)_{12}$-K (from 0 to 20 μM). The results, shown in Figure 6(B), indicate a dose-dependent antiviral effect of K-$(PNA)_{12}$-K, with a 50% cytopathic effect inhibitory concentration (IC_{50}) of about 16 μM.

In the same assay, a scrambled PNA with the sequence:

H-Lys-gacaacattgcg-Lys-NH_2

did not produce any inhibition of virus-induced cellular lysis.

Cellular Uptake of PNA and its Intracellular Localization

To enhance the efficiency in PNA delivery, many strategies were explored. These include microinjection, electroporation, co-transfection with DNA and permeabilization of cell membrane [31]. Since a positive charge will enhance the attraction of molecules to cell membrane, some attempts have been made by incorporating positively charged residues such as Lys or Arg to the PNA molecules to enhance the PNA delivery efficiency [32–36]. We reasoned that the presence of two

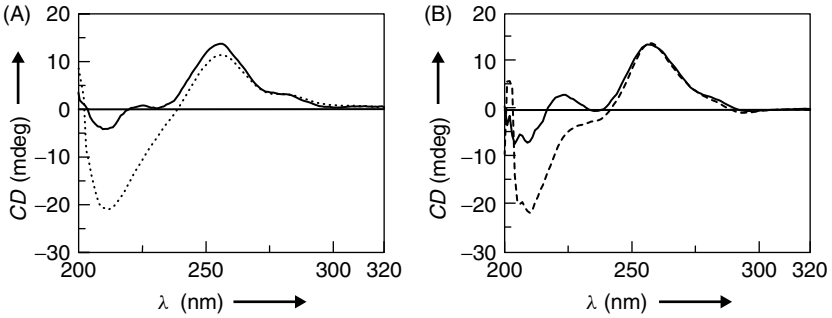

Figure 5 (A) SLD CD spectrum (continuous line); same, with the addition of $3C^{pro}$ (dotted line). (B) SLD + K-$(PNA)_{12}$-K (continuous line); same, with the addition of $3C^{pro}$ (dotted line).

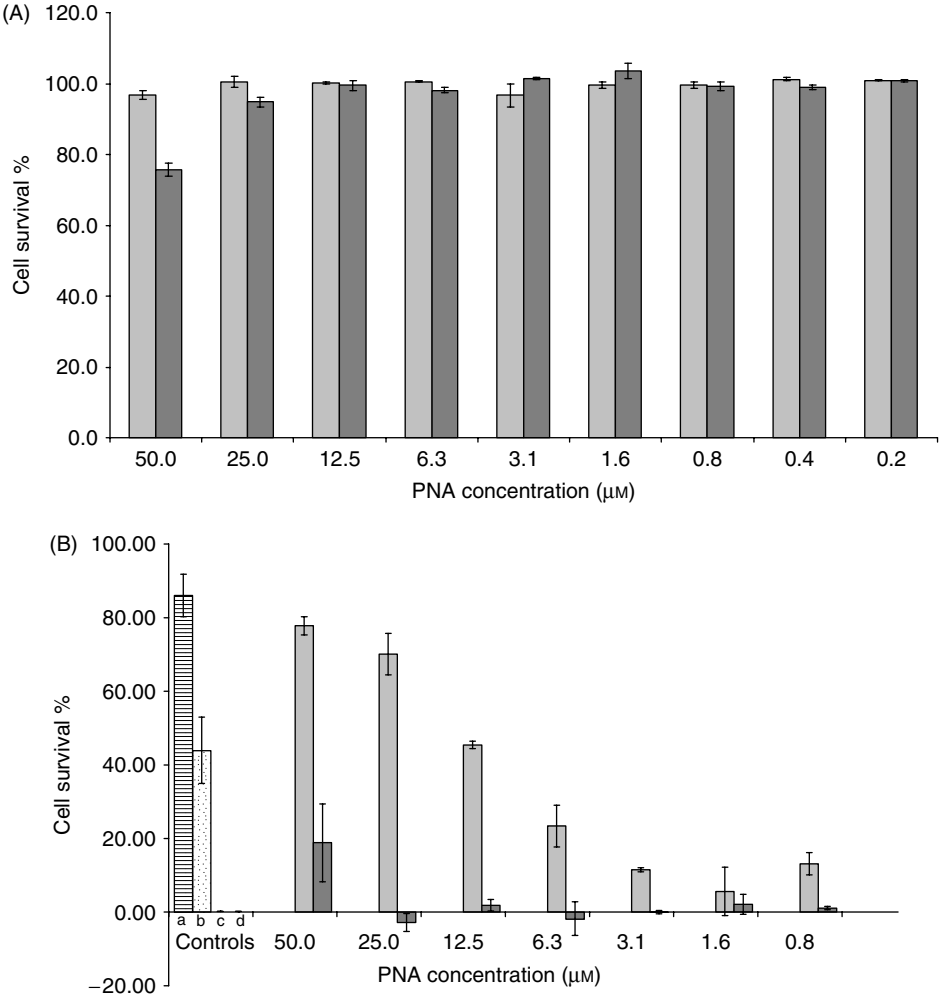

Figure 6 (A) CPE assay to assess the cytotoxic effect of K-$(PNA)_{12}$-K. The experiment was calibrated by assuming a 100% survival for untreated cells. Shown are the effect of K-$(PNA)_{12}$-K (light grey columns) and K-scrPNA_{12}-K (dark grey columns) at increasing concentrations. The standard deviation is also reported (three replicates for each concentration value). (B) CPE assay to test K-$(PNA)_{12}$-K anti-CVB3 activity. Increasing amounts of K-$(PNA)_{12}$-K where challenged against a fix amount of CVB3 virus and the survival of HeLa cells was subsequently assessed. K-$(PNA)_{12}$-K (light grey columns) shows an IC_{50} between 10 and 20 μM (interpolation: 16 μM). The scrambled PNA K-scrPNA_{12}-K (dark grey columns) does not show any protective effect. Controls (a: 100 microg/ml guanidinium chloride-inactivated virus; b: 32.5 microg/ml guanidinium chloride-inactivated virus; c and d, cells exposed to virus without any treatment) are also reported. Standard deviation from three independent experiments is also indicated.

Lys residues, which positively charge K-$(PNA)_{12}$-K, can attract PNA to the membrane, resulting in the crossing of the cell membrane. Therefore, we chose to deliver K-$(PNA)_{12}$-K by simply adding it to the culture medium. To monitor its uptake by cells, a β-Ala-fluorescein tag was added to K-$(PNA)_{12}$-K.

In a double staining experiment, HeLa cells were incubated with fluorescein-tagged K-$(PNA)_{12}$-K at 2 μM, the lowest concentration required for antiviral activity in coxsackievirus B3-infected cells (Figure 6). After 24 h incubation, HeLa cells were examined under the fluorescence microscope. The cells (identified by the blue fluorescence of their nucleus, Figure 7C) exhibited strong fluorescence, indicating PNA uptake (Figure 7B). The green halos in Figure 7(B) are indeed cells, and not just PNA aggregates, as it is evidenced by the fact that each halo corresponds to a blue-stained cellular nucleus (Figure 7D).

Finally, employing a trypan blue assay, the same cell viability was observed for untreated control cells and for cells treated either with FITC alone or with fluorescein-tagged K-$(PNA)_{12}$-K, respectively (data not shown).

In order to avoid the interference due to nuclear staining by Hoechst 33 258, we performed a staining experiment employing fluorescein-tagged K-$(PNA)_{12}$-K only. The conditions used were identical to those used for the double staining experiment. A sponge-like distribution of the fluorescein-tagged K-$(PNA)_{12}$-K was observed in the majority of the HeLa cells (Figure 8).

Staining of cytoplasmic regions appeared somewhat more intense as compared to nuclear staining: hence, PNA does not tend to accumulate in the nuclear compartment. Exclusion of PNA from the nucleus could be an important factor for the decrease of the active dose of the used PNA, since the CVB3 virus has a non-nuclear localization. However, artefacts due to the fixing procedure could not be excluded at this stage. We then repeated the experiments on living cells using a combined fluorescence/phase-contrast microscope. The cells appeared again fluorescent after treatment with the fluorescein-tagged K-$(PNA)_{12}$-K (Figure 9). Moreover, again the nuclear compartment seems to be excluded.

CONCLUSIONS

In conclusion, we described here the design, synthesis and activity of a short, specific PNA-based compound, referred to as K-$(PNA)_{12}$-K, able to specifically recognise the SLD in the 5′-cloverleaf of the genomic RNA from coxsackievirus B3. The administration of K-$(PNA)_{12}$-K is shown to block the viral-induced cellular lysis with an IC_{50} of 16 μM, without cytotoxic effects.

To our knowledge, there is only one other RNA virus that was shown to be sensitive to treatment by PNA, namely, HIV-1 [37–39]. In addition, we want to stress that this IC_{50} value is in the same range as those of other very different compounds able to block CVB3 infection, e.g. the capsid-binder SCH 38 057 [40].

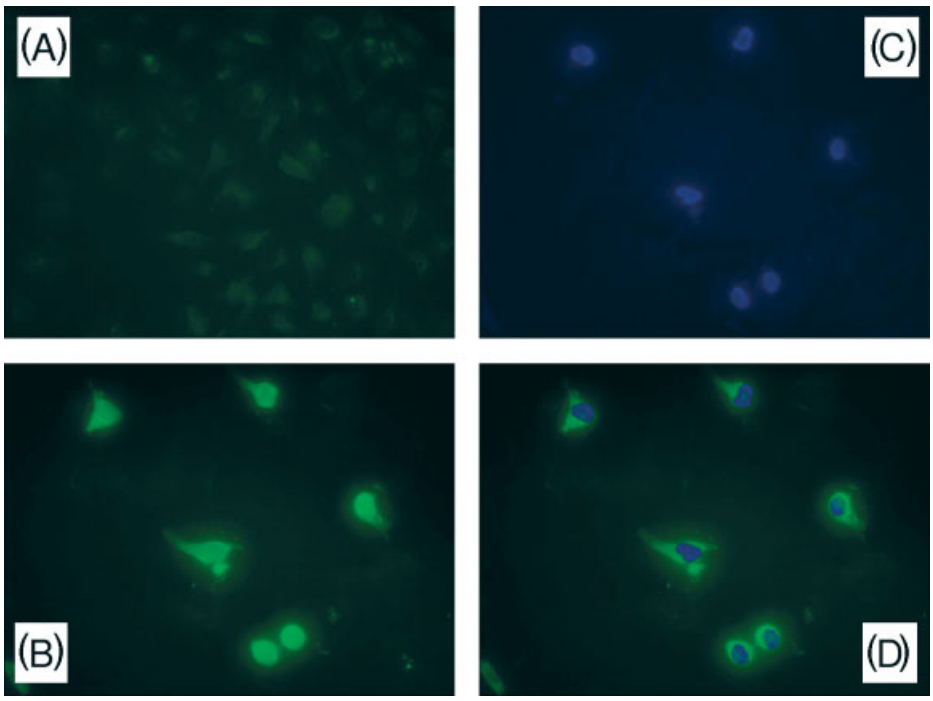

Figure 7 Fluorescence microscopy of HeLa cells incubated with 2 μM FITC only (A); the fluorescence signal of fluorescein-tagged K-$(PNA)_{12}$-K (B); the signal from the nuclear counter-stain by Hoechst 33 258 (C); overlay of images of Hoechst 33 258 and fluorescein-tagged K-$(PNA)_{12}$-K (D).

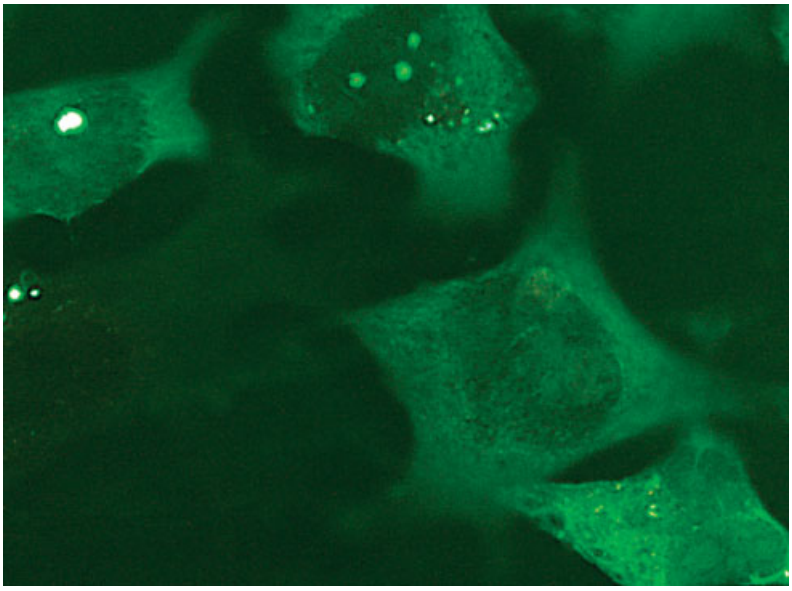

Figure 8 Fluorescence microscopy of HeLa cells incubated with 2 μM fluorescein-tagged K-$(PNA)_{12}$-K.

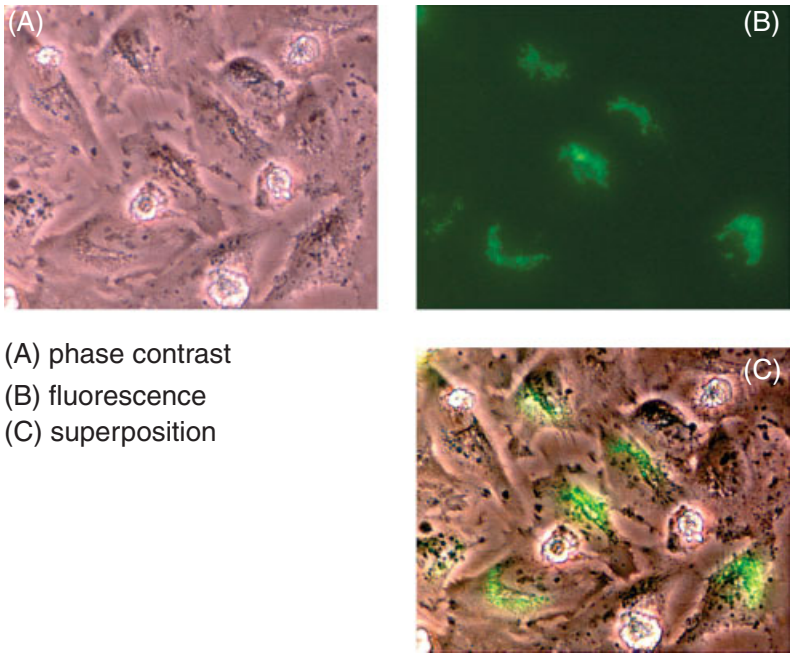

Figure 9 Combined contrast/fluorescence microscopy on living HeLa cells incubated with 2 μM fluorescein-tagged K-$(PNA)_{12}$-K.

Our results also indicate that K-$(PNA)_{12}$-K is able to enter the HeLa cells without further additions of transporter/cargo moieties, thus simplifying the production of large quantities of such a compound for a potential therapeutic use, and localizes in the cytoplasm, which is an useful property in light of the proposed targeting of a cytoplasmic virus.

Acknowledgements

We thank S. Häfner and G. Perretta for their excellent technical assistance.

REFERENCES

1. Dean NM. Functional genomics and target validation approaches using antisense oligonucleotide technology. *Curr. Opin. Biotechnol.* 2001; **12**: 622–625.
2. Gao WY, Han FS, Storm C, Egan W, Cheng YC. Phosphorothioate oligonucleotides are inhibitors of human DNA polymerases and RNase H: implications for antisense technology. *Mol. Pharmacol.* 1992; **41**: 223–229.
3. Armitage BA. The impact of nucleic acid secondary structure on PNA hybridization. *Drug Discov. Today* 2003; **8**: 222–228.
4. Nielsen PE. Peptide nucleic acids as therapeutic agents. *Curr. Opin. Struct. Biol.* 1999; **9**: 353–357.
5. Rebuffat AG, Nawrocki AR, Nielsen PE, Bernasconi AG, Bernal-Mendez E, Frey BM, Frey FJ. Gene delivery by a steroid-peptide nucleic acid conjugate. *FASEB J.* 2002; **16**: 1426–1428.

6. Lewis MR, Jia F, Gallazzi F, Wang Y, Zhang J, Shenoy N, Lever SZ, Hannink M. Radiometal-labeled peptide-PNA conjugates for targeting bcl-2 expression: preparation, characterization, and in vitro mRNA binding. *Bioconjug. Chem.* 2002; **13**: 1176–1180.
7. Eriksson M, Nielsen PE, Good L. Cell permeabilization and uptake of antisense peptide-peptide nucleic acid (PNA) into Escherichia coli. *J. Biol. Chem.* 2002; **277**: 7144–7147.
8. Svanvik N, Nygren J, Westman G, Kubista M. Free-probe fluorescence of light-up probes. *J. Am. Chem. Soc.* 2001; **123**: 803–809.
9. Friebe P, Lohmann V, Krieger N, Bartenschlager R. Sequences in the 5′ nontranslated region of hepatitis C virus required for RNA replication. *J. Virol.* 2001; **75**: 12 047–12057.
10. Becher P, Orlich M, Thiel HJ. Mutations in the 5′ nontranslated region of bovine viral diarrhea virus result in altered growth characteristics. *J. Virol.* 2000; **74**: 7884–7894.
11. Kusov YY, Gauss-Muller V. In vitro RNA binding of the hepatitis A virus proteinase 3C (HAV 3Cpro) to secondary structure elements within the 5′ terminus of the HAV genome. *RNA* 1997; **3**: 291–302.
12. Kim KH, Hemenway C. The 5′ nontranslated region of potato virus X RNA affects both genomic and subgenomic RNA synthesis. *J. Virol.* 1996; **70**: 5533–5540.
13. Basso J, Dallaire P, Charest PJ, Devantier Y, Laliberte JF. Evidence for an internal ribosome entry site within the 5′ nontranslated region of turnip mosaic potyvirus RNA. *J. Gen. Virol.* 1994; **75**(Pt 11): 3157–3165.
14. Lyons T, Murray KE, Roberts AW, Barton DJ. Poliovirus 5′-terminal cloverleaf RNA is required in cis for VPg uridylylation and the initiation of negative-strand RNA synthesis. *J. Virol.* 2001; **75**: 10 696–10708.
15. Richards OC, Ehrenfeld E. Poliovirus RNA replication. *Curr. Top. Microbiol. Immunol.* 1990; **161**: 89–119.
16. Wimmer E, Kuhn RJ, Pincus S, Yang CF, Toyoda H, Nicklin MJ, Takeda N. Molecular events leading to picornavirus genome replication. *J. Cell Sci. Suppl.* 1987; **7**: 251–276.
17. Santti J, Vainionpaa R, Hyypia T. Molecular detection and typing of human picornaviruses. *Virus Res.* 1999; **62**: 177–183.
18. Wang QM. Protease inhibitors as potential antiviral agents for the treatment of picornaviral infections. *Prog. Drug Res.* 2001; Special issue, **52**: 229–253.
19. Kong JS, Venkatraman S, Furness K, Nimkar S, Shepherd TA, Wang QM, Aube J, Hanzlik RP. Synthesis and evaluation of peptidyl Michael acceptors that inactivate human rhinovirus 3C protease and inhibit virus replication. *J. Med. Chem.* 1998; **41**: 2579–2587.
20. Andino R, Rieckhof GE, Baltimore D. A functional ribonucleoprotein complex forms around the 5′ end of poliovirus RNA. *Cell* 1990; **63**: 369–380.
21. Andino R, Rieckhof GE, Trono D, Baltimore D. Substitutions in the protease (3Cpro) gene of poliovirus can suppress a mutation in the 5′ noncoding region. *J. Virol.* 1990; **64**: 607–612.
22. Zell R, Sidigi K, Bucci E, Stelzner A, Gorlach M. Determinants of the recognition of enteroviral cloverleaf RNA by coxsackievirus B3 proteinase 3C. *RNA* 2002; **8**: 188–201.
23. Ohlenschlager O, Wohnert J, Bucci E, Seitz S, Hafner S, Ramachandran R, Zell R, Gorlach M. The structure of the stemloop D subdomain of coxsackievirus B3 cloverleaf RNA and its interaction with the proteinase 3C. *Structure* 2004; **12**: 237–248.
24. Hingamp P, van den Broek AE, Stoesser G, Baker W. The EMBL nucleotide sequence database. Contributing and accessing data. *Mol. Biotechnol.* 1999; **12**: 255–267.
25. Skripkin EA, Jacobson AB. A two-dimensional model at the nucleotide level for the central hairpin of coliphage Q β RNA. *J. Mol. Biol.* 1993; **233**: 245–260.
26. Pace CN, Vajdos F, Fee L, Grimsley G, Gray T. How to measure and predict the molar absorption coefficient of a protein. *Protein Sci.* 1995; **4**: 2411–2423.
27. Schmidtke M, Schnittler U, Jahn B, Dahse H, Stelzner A. A rapid assay for evaluation of antiviral activity against coxsackievirus B3, influenza virus A, and herpes simplex virus type 1. *J. Virol. Methods* 2001; **95**: 133–143.
28. Eriksson M, Nielsen PE. PNA-nucleic acid complexes. Structure, stability and dynamics. *Q. Rev. Biophys.* 1996; **29**: 369–394.
29. Isernia C, Bucci E, Leone M, Zaccaro L, Di Lello P, Digilio G, Esposito S, Saviano M, Di Blasio B, Pedone C, Pedone PV, Fattorusso R. NMR structure of the single QALGGH zinc finger domain from the Arabidopsis thaliana SUPERMAN protein. *Chem Biochem* 2003; **4**: 171–180.
30. Sosnick TR, Fang X, Shelton VM. Application of circular dichroism to study RNA folding transitions. *Meth. Enzymol.* 2000; **317**: 393–409.
31. Koppelhus U, Nielsen PE. Cellular delivery of peptide nucleic acid (PNA). *Adv. Drug Deliv. Rev.* 2003; **55**: 267–280.
32. Wang G, Xu XS. Peptide nucleic acid (PNA) binding-mediated gene regulation. *Cell Res.* 2004; **14**: 111–116.
33. Filipovska A, Eccles MR, Smith RA, Murphy MP. Delivery of antisense peptide nucleic acids (PNAs) to the cytosol by disulphide conjugation to a lipophilic cation. *FEBS Lett.* 2004; **556**: 180–186.
34. Sazani P, Kang SH, Mauer MA, Wie C, Dillman J, Summerton J, Manoharan M, Kole R. Nuclear antisense effects of neutral, anionic and cationic oligonucleotide analogs. *Nucleic Acids Res.* 2001; **29**: 3965–3974.
35. Kole R, Williams T, Cohen L. RNA modulation, repair and remodeling by splice switching oligonucleotides. *Acta Biochim. Pol.* 2004; **51**: 373–378.
36. Moulton H, Moulton JD. Peptide-assisted delivery of steric-blocking antisense oligomers. *Curr. Opin. Mol. Ther.* 2003; **5**: 123–132.
37. Koppelhus U, Zachar V, Nielsen PE, Liu X, Eugen-Olsen J, Ebbesen P. Efficient in vitro inhibition of HIV-1 gag reverse transcription by peptide nucleic acid (PNA) at minimal ratios of PNA/RNA. *Nucleic Acids Res.* 1997; **25**: 2167–2173.
38. Terreux R, Pairot S, Cabrol-Bass D, Patino N, Condom R. Interaction of new PNA-based molecules with TAR RNA of HIV-1: molecular modelling and biological evaluation. *J. Mol. Graph.* 2001; **19**: 579–585.
39. Lee R, Kaushik N, Modak MJ, Vinayak R, Pandey VN. Polyamide nucleic acid targeted to the primer binding site of the HIV-1 RNA genome blocks in vitro HIV-1 reverse transcription. *Biochemistry* 1998; **37**: 900–910.
40. Rozhon E, Cox S, Buontempo P, O'Connell J, Slater W, De Martino J, Schwartz J, Miller G, Arnold E, Zhang A. SCH 38057: a picornavirus capsid-binding molecule with antiviral activity after the initial stage of viral uncoating. *Antiviral Res.* 1993; **21**: 15–35.

